FISEVIER

Contents lists available at ScienceDirect

Journal of Volcanology and Geothermal Research

journal homepage: www.journals.elsevier.com/journal-of-volcanology-and-geothermal-research





Paleomagnetism and age of the Leucite Hills Volcanic complex, Wyoming: Implications for eruptive history, landscape evolution, and the geomagnetic instability timescale (GITS)

J.T. Welsh ^a, J.M. Feinberg ^{a,b,*}, E. Schneider ^{a,b}, J.M. Pares ^c, B.R. Jicha ^d, B.S. Singer ^d, A.R. Carroll ^d

- a Department of Earth & Environmental Sciences, University of Minnesota, 116 Church Street SE, Minneapolis 55455, MN, United States of America
- b Institute for Rock Magnetism, University of Minnesota, 116 Church Street SE, Minneapolis 55455, MN, United States of America
- ^c Centro Nacional de Investigación sobre la Evolución Humana, Burgos, Spain
- d Department of Geoscience, University of Wisconsin-Madison, 1215 W Dayton St, Madison, Madison 53706, WI, United States of America

ARTICLE INFO

Keywords: Lamproite Paleomagnetism 40 Ar/39 Ar geochronology Kamikatsura geomagnetic excursion Leucite Hills Volcanic complex

ABSTRACT

The Leucite Hills Volcanic Field, southwest Wyoming comprises two dozen volcanic features including necks, flows, dikes, and plugs. It has been the focus of many petrologic studies as its volcanic and shallow intrusive rocks are one of the only surficial manifestations of ultrapotassic lamproite. We build on paleomagnetic findings of Sheriff and Shive (1980) by providing further paleomagnetic data from the Boars Tusk dike and Black Rock flows. We also characterize the magnetic mineral assemblage of these lamproites. Principal component analysis of alternating field (AF) and thermal demagnetization data indicate that the dike and breccias of Boars Tusk record a reversed magnetic polarity and the Black Rock lava records a normal polarity, both consistent with previous findings. This recording is typically carried by minerals with coercivities >15 mT and susceptibility measurements indicate magnetite, maghemite, and titanomagnetite as likely magnetic carriers. AF and thermal demagnetization experiments evince secondary magnetizations held by lower coercivity grains, likely caused by lightning strikes. 40Ar/39Ar incremental heating experiments from Boars Tusk and Black Rock give plateau ages of ~ 2500 ka and ~ 900 ka, respectively. Recent advances in the chronology of geomagnetic field reversals and excursions during the Quaternary permit integration of the Boars Tusk dike into the lower Matuyama chron, whereas the Black Rock lavas most probably record the Kamikatsura excursion. Notably, Black Rock records high inclinations that suggest the short-lived excursion achieved a full geomagnetic reversal, something not observed at other localities recording the Kamikatsura excursion. The Leucite Hills offer further opportunities to refine the Quaternary geomagnetic instability time scale (GITS), and to improve understanding of the eruptive and geomorphic evolution of this unusual volcanism.

1. Introduction

The Leucite Hills volcanic field (LHVF) is located in southwest Wyoming, just north of the city of Rock Springs (Fig. 1). The field covers an area of $\sim\!2000\,\mathrm{km}^2$ and contains roughly two dozen volcanic features including necks, flows, plugs, and dikes (Lange et al., 2000) made of lamproite, an ultrapotassic mafic rock that is compositionally extreme (Carmichael, 1967). The volcanic rocks of the LHVF have been of interest over the past century and a half for several reasons, including their potential as a source of potash and peridot for agricultural, industrial,

and aesthetic purposes (Hausel, 2006). Today, the LHVF offers an interesting locality for scientific study. Its features present opportunities to: (1) evaluate and refine the Quaternary geomagnetic instability time scale (GITS) first developed by Singer et al. (1999), with expanded updates in Singer (2014) and Channell et al. (2020), (2) determine the rate of post-emplacement erosion, and (3) gain a deeper understanding of the magnetic mineralogy, source, and eruptive behavior of this uncommon magma type.

Various geochronologic methods have been used to constrain the history of the Leucite Hills. Many of the features in the LHVF were the

E-mail address: feinberg@umn.edu (J.M. Feinberg).

^{*} Corresponding author at: Department of Earth & Environmental Sciences, University of Minnesota, 116 Church Street SE, Minneapolis 55455, MN, United States of America.

focus of paleomagnetic measurements performed more than 4 decades ago (Sheriff and Shive, 1980) and Lange et al. (2000) used $^{40}{\rm Ar}/^{39}{\rm Ar}$ geochronology to date many of the same features. While the ages and paleodirectional data acquired from some of these features agree with the GPTS, others do not and warrant further investigation. We focus on two features: the Boars Tusk dike and Black Rock lava flows. Sheriff and Shive (1980) found that Boars Tusk is reversely magnetized with a declination and inclination of 165° and -50°, respectively. Lange et al. (2000) report an $^{40}{\rm Ar}/^{39}{\rm Ar}$ age of 2230 \pm 30 ka (2 σ analytical uncertainty) for Boars Tusk, allowing the reversed polarity of the feature to be correlated into the lower Matuyama reversed chron, also known as chron C1r in Cande and Kent (1992, 1995) and Ogg (2020). In the same studies, Black Rock was found to be normally magnetized with a declination and inclination of 21° and 57° and with an $^{40}{\rm Ar}/^{39}{\rm Ar}$ age of 1320

 \pm 70 ka. Although an age of 1320 ka should place these lavas in the upper portion of C1r, the normal inclination indicates that one of the polarity excursions identified in lava flows by Singer et al. (1999), and reviewed by Laj and Channell (2007), Singer (2014), Channell et al. (2020), and Ogg (2020) is recorded. We re-examine the paleomagnetism of these two features using updated protocols, provide new ⁴⁰Ar/³⁹Ar dates from multiple grain sizes of phlogopite to augment previous radioisotopic dating by Lange et al. (2000) and propose that Black Rock lavas record the Kamikatsura excursion that has been recognized in tuffs near Osaka, Japan, lava flows on Tahiti and Maui, as well as in deep ocean sediment cores (Singer, 2014; Channell et al., 2020). Moreover, we provide a detailed characterization of the magnetic mineralogy of the lamproite at Boars Tusk and the breccia that surrounds its base, which helps provide insight about the timing of remanence acquisition. Sheriff and Shive (1980) conclude that the remanence was held by a Ti-poor spinel with a composition close to magnetite based on AF demagnetization to 40 mT and thermomagnetic experiments. We use hysteresis loops, backfield curves, susceptibility as a function of temperature and electron microprobe analyses to better characterize the remanence carriers in these rocks and their potential as paleomagnetic recorders. We also provide quantitative geochemical measurements and backscatter electron microprobe maps of the silicate minerals in the Boars Tusk dike, including the phlogopite that is the focus of our ⁴⁰Ar/³⁹Ar dating.

2. Geologic context

The volcanic features of the Leucite Hills are surrounded by and erupted through a thick sequence of Cretaceous and Tertiary sedimentary rocks on the NE margin of the Rock Springs Anticline (Lange et al., 2000). The Wyoming Craton constitutes the basement rock and has been stable since 2.6-2.7 Ga (Houston et al., 1993). Roughly 100 km to the south lies the Chevenne belt, an ancient tectonic suture that marks the boundary between the Wyoming Craton and the Colorado Plateau (Lange et al., 2000). Many of the volcanic features of the Leucite Hills are aligned parallel to the nearby Farson lineament. Boars Tusk is the westernmost feature in the Leucite Hills and comprises an eroded northsouth oriented wyomingite dike that bisects the neck into two spires of volcanic breccia that crop out above the top of the dike. The breccia contains xenoliths of country rocks with grain sizes ranging from sand to meter-sized boulders. The breccia can be separated into two units based on the density of xenoliths (Fig. 2) (Ogden, 1979). At the base of the neck, there is a cone of talus that is approximately 60 m tall and fully covers the contact between the volcanic rock and the surrounding country rock (Schultz and Cross, 1912).

Black Rock is the easternmost feature in the Leucite Hills and is a roughly circular mesa that covers roughly 48,000 m² and rises ~ 140 m above the valley bottom. The mesa top is a \sim 30m thick layer of lava flows which covers roughly 70 m of sediments. The top of the mesa gently slopes downwards toward the mesa center. Like Boars Tusk, a slope of talus rises to the edges of the volcanic rock covering the contact between the volcanic feature and the country rock. Some portions of the exposed volcanic rock are porous and scoriaceous while others are denser and more massive. There are alternating bands of these two general lithologies, which become a prominent feature near the top (Schultz and Cross, 1912). The LHVC magmas are thought to have formed from the melting of a ~ 2.3 Ga vein fraction of mantle below the Rock Springs area (Lange et al., 2000). The vein reflects multiple metasomatic events (one between 1.0 and 2.8 Ga and another <100 Ma) that produced an extreme mantle composition, that in turn is reflected in the composition of the rocks of the Leucite Hills (Mirnejad and Bell, 2006). The mechanism for the heating which caused the formation of these magmas is still uncertain, though multiple hypotheses have been proposed (Mirnejad and Bell, 2006). The conventional interpretation

Map of Leucite Hills Volcanic Field

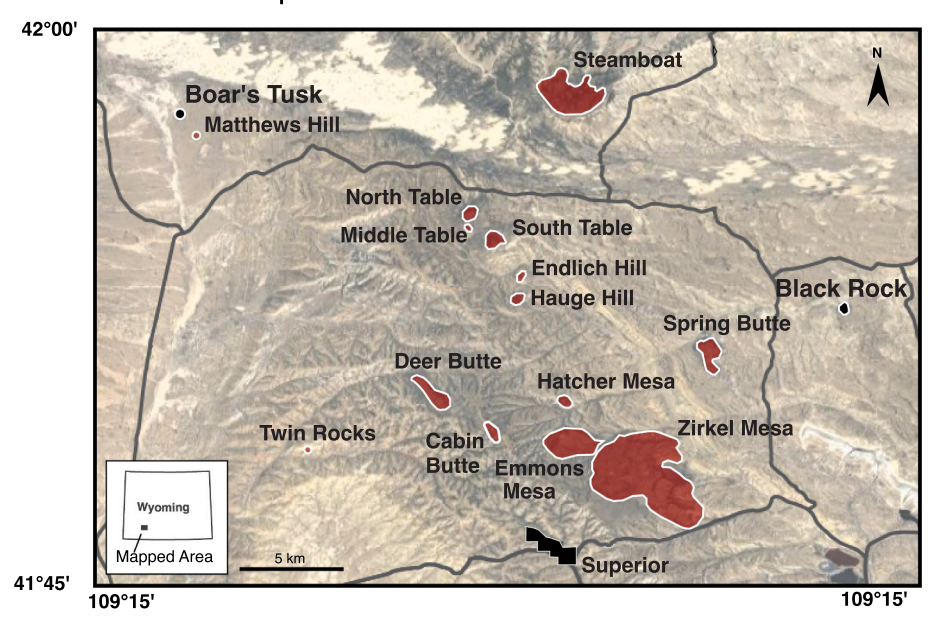


Fig. 1. Map of the Leucite Hills volcanic field with locations of volcanic features, the town of Superior and roadways within the area. The inset provides the study's location within the state of Wyoming.

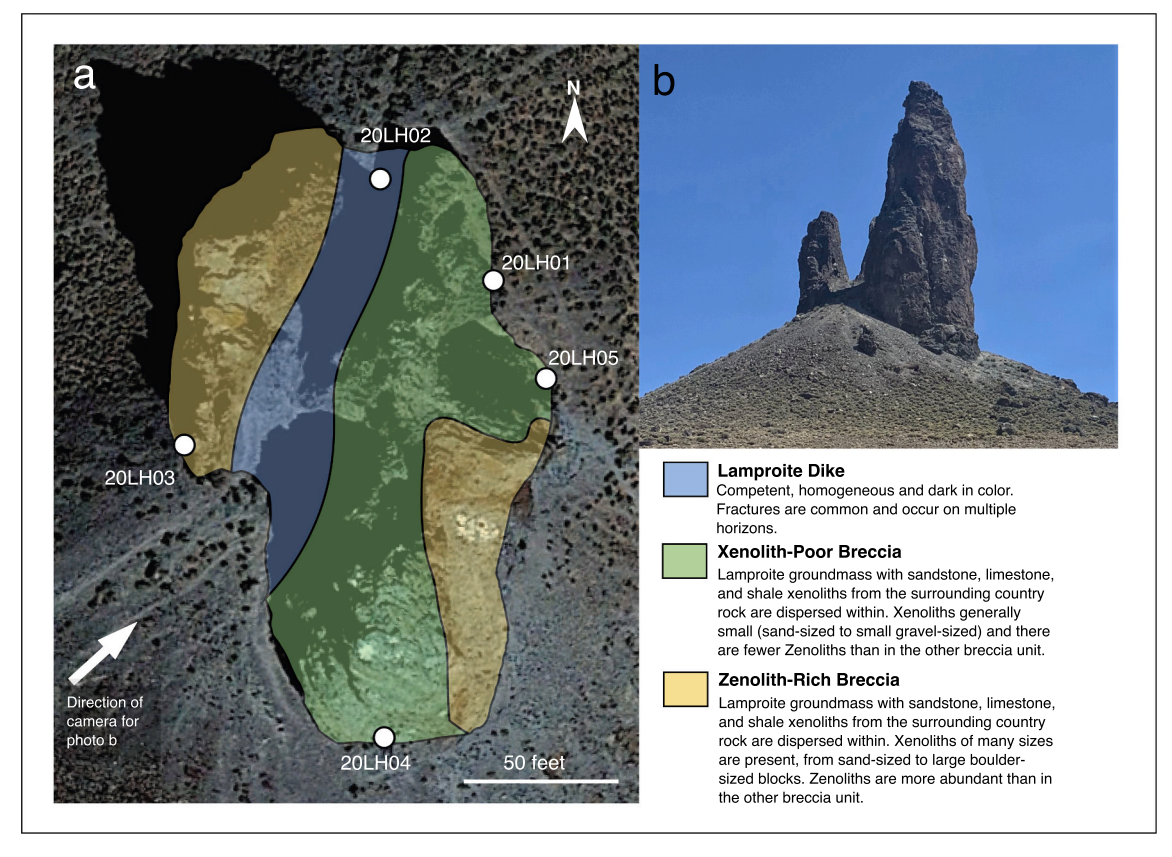


Fig. 2. (a) Map of Boars Tusk showing geologic units and sampling sites. Geologic units described below image b. (b) Image of Boars Tusk showing its two spires and talus cone. The lamproite dike identified as blue in (a) follows the notch between the spires. Light areas that can be seen partway up the spires are country rock xenoliths. (For interpretation of the references to colour in this figure legend, the reader is referred to the web version of this article.)

invokes the shallow subduction of the Farallon plate and the concomitant metasomatic generation of mantle-derived magmas (Lipman et al., 1980; Bird, 1984). However, this model is problematic in that it requires the subducting slab to remain intact and exceptionally shallow while extending nearly 1500 km inland from the subducting trench while also simultaneously subducting below the thick Wyoming Craton. Alternatively, the mantle could have been heated at the fringe of the Quaternary Yellowstone hotspot, which is coeval with emplacement of the Leucite Hills. However, the hotspot is over 300 km away during this time. Finally, it is possible that magma formation occurred as the culmination of mantle upwelling associated with back-arc extension and lithospheric thinning (Eggler et al., 1988). Lange et al. (2000) suggest that features in the LHVC range in age from ~ 3 to <1 Ma. The Leucite Hills rocks are lamproite, solidified from a rare ultrapotassic mafic magma. Boars Tusk and Black Rock are composed of a specific type of lamproite characterized by crystals of phlogopite in a groundmass of leucite, diopside, apatite, and occasionally glass (Schultz and Cross, 1912) that is known as wyomingite in regional nomenclature (Cross, 1897; Carmichael, 1967) or diopside-leucite-phlogopite lamproite when using the more generalized nomenclature created for lamproites (e.g., Woolley et al., 1996). Interestingly, Carmichael (1967) found no evidence of FeTi oxide minerals in wyomingite from the Leucite Hills, which helps explain the unusually weak magnetization of these rocks.

3. Methods

3.1. Sample collection

Five sites were chosen at Boars Tusk based on competency of the rock, lack of xenoliths, good spatial distribution, and the feasibility of drilling (Fig. 2). Four of these sites sample breccia and one site samples

the lamproite dike that forms the core of the structure. Four sites were chosen at Black Rock based on proximity to sampling locations used by Lange et al. (2000). A gas-powered drill was used to cut seven to ten 2.5 cm diameter core samples at each location, which were oriented in-situ using a sun compass orienting tool before core removal. A block sample of the dike at Boars Tusk was also collected for $^{40}{\rm Ar}/^{39}{\rm Ar}$ experiments at the WiscAr Lab at the University of Wisconsin-Madison. Boars Tusk cores were returned to the Institute for Rock Magnetism at the University of Minnesota - Twin Cities, and Black Rock cores were returned to Paleomagnetism Laboratory of the University of Michigan, where paleomagnetic and rock magnetic characterization measurements were conducted.

3.2. Paleodirectional methods

3.2.1. Boars Tusk

The cores were cut in 5 mm thick specimens using a brass-blade rock saw. Specimens were sanded on all sides to remove any possible metal contamination from the saw blades and/or core drill bits. Specimens were selected preferentially from areas within the cores with fewer xenoliths and fractures. 50 specimens were analyzed using alternating field and thermal demagnetization. A D-Tech D-2000 was used for AF demagnetization and an ASC Scientific TD48-SC furnace was used for thermal demagnetization. Magnetic measurements were made using a 2G Enterprises 760-R SQUID magnetometer. All measurements were made within a shielded room with a background field between 200 and 400 nT. Sixteen demagnetization steps between 0 and 170 mT were used for the alternating field demagnetization and 16 steps between 25 and 690 °C were used for the thermal demagnetization. Low field magnetic susceptibility was measured after each thermal demagnetization step to monitor mineral alteration using a Magnon Variable Frequency

Susceptibility Meter operated at 300 A/m with a frequency of 465 Hz. Principal and secondary components of magnetization were identified using principal component analysis in PuffinPlot (Lurcock and Wilson, 2012).

3.2.2. Black Rock

Cores were cut into 2.1 cm specimens in the laboratory. Natural Remanent Magnetization (NRM) was measured with a 2G SQUID magnetometer housed in a magnetic field-free room at the Paleomagnetism Laboratory of the University of Michigan. Progressive thermal demagnetization carried out in an ASC furnace was used to isolate the magnetic components of the samples, although a couple of specimens were AF demagnetized. A total of 60 specimens were analyzed, 4 through AF demagnetization and 56 through thermal demagnetization. Least-squares fits to the linear demagnetization trajectory for the Characteristic Remanent Magnetization (ChRM) in each sample were made by principal component analysis (Kirschvink, 1980), guided by visual inspection of orthogonal demagnetization plots (Zijderveld, 1967).

3.3. Magnetic mineralogy methods

3.3.1. Low field susceptibility as a function of temperature

Representative samples from each site at Boars Tusk were crushed to a coarse powder for measurements of low field susceptibility as a function of temperature using a KLY-2 KappaBridge AC Susceptibility Bridge with a C2 furnace. Each powdered sample was placed in a quartz test tube and weighed prior to measurement. All samples were measured in air. Susceptibility was measured every 2–4 $^{\circ}\text{C}$ during heating from room temperature (27 $^{\circ}\text{C}$) to 690 $^{\circ}\text{C}$ and during subsequent cooling back to room temperature. Curie temperatures were found using the first derivative method after smoothing to reduce any noise within the data.

3.3.2. Vibrating sample magnetometry

Representative specimens were selected from the dike and the breccia at Boars Tusk for hysteresis and backfield curve measurements using a Princeton Measurements Micromag Vibrating Sample Magnetometer. Hysteresis loops were collected on unheated specimens up to peak fields of 1.1 T and analyzed using the approach of Jackson and Solheid (2010). Backfield curves were collected using logarithmically spaced data and coercivity spectra were examined using Maxbauer et al. (2016).

3.4. Electron microprobe

Representative specimens were selected for electron microprobe analyses from the dike (20LH02-01 A) and breccia (20LH03-01 A) at Boars Tusk. Specimens were polished to 0.25 μ m. Images and measurements were collected using a JEOL JXA-8350FPlus Electron Probe Microanalyzer at the University of Minnesota. Energy dispersive spectrometry (EDS) measurements were collected using a Thermo Noran System 7 EDS with Ultradry-SDD detector and the complete Pathfinder software package. The accelerating voltage and emission current used during EDS measurements were 15.0 kV and 65.8 μ A, respectively. Wavelength dispersive spectrometry (WDS) measurements were collected with varying analytical conditions based on the needs of particular minerals (Table 1).

3.5. 40Ar/39Ar methods

Hand-picked phlogopite crystals from the Boars Tusk and Black Rock samples were wrapped in Al foil, placed in 2.5 cm Al disks, and irradiated in the cadmium-lined in-core tube at the Oregon State University reactor. The 1.1864 Ma Alder Creek sanidine (Jicha et al., 2016) was used as a neutron fluence monitor. $^{40}\mbox{Ar/}^{39}\mbox{Ar}$ analyses were conducted in the WiscAr Laboratory at the University of Wisconsin-Madison. Single

Electron microprobe results and analytical conditions

Mineral Phase	SiO_2	TiO_2	SiO_2 TiO_2 Al_2O_3 MgO	MgO	FeO	MnO	Na_2O	CaO	Cr_2O_3	K_2O	BaO	P_2O_5	Total	grains (n)	measurements per grain	voltage	current	pec
Homblende	39.85	9.37	9.33	18.23	8.99	60.0	0.42	0.05	0.03	9.62	1.66	ı	97.64	4	12	15	20	
Phlogopite (from dike)	41.5	2.14	12.36	25.17	3.04	0.02	0.23	0.03	0.83	10.53	0.38	I	96.22	10	13	15	20	
Phlogopite (from breccia)	41.7	2.09	11.76	25.33	3.56	0.03	0.16	0.02	0.26	10.64	0.38	I	95.93	10	17	15	20	
Diopside	54.31	0.67	0.24	17.49	3.24	0.11	0.33	24.29	0.02	0.02	0.01	I	100.72	7	14	15	20	
Albite	26.87	0.19	21.43	0.5	2.18	ı	11.66	0.1	1	1.55	1	ı	94.47	œ	21	15	10	
Apatite	0.54	ı	ı	0.27	0.28	0.05	I	53.46	1	ı	1	40.8	95.4	œ	16	15	20	

compositional measurements are reported as weight percent oxides; the accelerating voltage is in units of kV; current is in units of nA, and beam diameter is in units of µm.

phlogopite crystals were incrementally heated with a 55 W CO $_2$ laser and the gas was cleaned via exposure to two SAES GP50 getters in series (both at 50 W/400 $^{\circ}$ C) for 90 s each and to an ARS cryotrap (at $-125\,^{\circ}$ C) for another 60 s. Isotopic analyses were done using a Nu Instruments Noblesse mass spectrometer. Sample analyses consisted of a continuous measurement for ~ 1000 seconds, whereas blank and gas cocktail measurements were made with a peak hop routine described in Jicha et al. (2016). $^{40}\text{Ar}/^{39}\text{Ar}$ ages are calculated using the decay constants of Min et al. (2000), and reported with 2σ analytical uncertainties, which include the uncertainty on the J value.

4. Results

4.1. Paleodirectional analyses

4.1.1. Boars Tusk

A reliable characteristic remanent magnetization (ChRM) was obtained for all cores using alternating field (AF) demagnetization. Calculated Fisher mean declination and inclination values for each site are reported in Table 2. Individual specimen directions were accepted when the maximum angular deviation (MAD) is below 10° for AF demagnetization and 20° for thermal demagnetization. 48 of 49 specimens met the acceptance criteria. Fisher mean directions for AF demagnetization were accepted when k >50, and α_{95} <14°. The AF demagnetization data for site 20LH03 (xenolith-rich breccia) did not meet these criteria but was included due to its directions being coincident with other sites. Its thermal demagnetization data were noisier than those at other sites, likely introducing greater error. All sites were included with caution. AF demagnetization revealed that most Boars Tusk specimens had a secondary component of magnetization that was removed by fields of 15 mT (Fig. 3). The directions obtained from the higher-coercivity components are consistent within each site and between all sites, leading to the conclusion that these are reliable ChRMs. The Fisher mean declination and inclination for these high coercivity directions is 177.2° and -53.6° , respectively. Secondary components were consistent within each site, but not between sites. These low coercivity directions generally have a mean direction with low angle inclination; some are normally magnetized while others are reversely magnetized. Fig. 4 (a) and (b) show the distribution of high coercivity directions and low coercivity directions, respectively. Of the 26 specimens demagnetized using alternating fields, 11 did not lose all of their magnetization at high field strengths, indicating the presence of a high coercivity mineral such as hematite.

Thermal demagnetization data was significantly noisier than the AF demagnetization data, but directions could still be determined for most specimens. Site means for thermal data are reported in Table 2. Like the low coercivity AF components, the directions derived from thermal demagnetization were consistent within sites, but not between sites. Directions isolated from low coercivity AF and thermal demagnetization were generally coincident at each site. Fig. 4 (c) shows the distribution of thermal directions. Unlike the alternating field data, the thermal data did not show secondary components of magnetization. This may be partly attributable to the increased noise in the thermal data, but even in the clearest demagnetization data, no secondary component is present. This suggests that while the grains holding the secondary magnetization have lower coercivities than those holding the ChRM, the thermal unblocking spectra for the two components overlap significantly. The average natural remanent magnetization (NRM) intensity is listed in Table 2 by site and lithology (dike vs. breccia). The suite averaged NRM is 2.6×10 –5 Am²kg⁻¹, or $\sim 6.7 \times 10^{-2}$ Am⁻¹. The NRM values are relatively consistent between sites of the same lithology, however the average NRM value for the dike samples ($\sim 5 \times 10^{-5} \text{ Am}^2 \text{kg}^{-1}$) is an order of magnitude higher than that of the breccia samples (\sim 5 \times 10⁻⁶ Am²kg⁻¹). These values are quite low for volcanic features, as they are \sim 4 - 5 orders of magnitude lower than the average NRM value of oceanic sheeted dikes (Dunlop and Özdemir, 1997).

4.1.2. Black Rock

Calculated Fisher mean declination and inclination values for each site are reported in Table 2. Directions from individual specimens were

Table 2
Paleomagnetic data by site.

Treatment/ Grouping	Site	Site Avg NRM	Declination	Inclination	a ₉₅	k	n/N
Units		$Am^2 kg^{-1}$	۰	۰	•		
AF High Coercivity	20LH01	1.77E-05	177.7	-50.6	11.6	115	3/5
AF High Coercivity	20LH02	9.37E-05	189.8	-54.3	13.2	49.5	4/6
AF High Coercivity	20LH03	7.49E-06	188.7	-53.7	19.1	16.9	5/5
AF High Coercivity	20LH04	5.90E-06	169.1	-45.8	6.7	131.5	5/5
AF High Coercivity	20LH05	3.95E-06	163	-60.5	5.8	177.4	5/5
BT Suite Average		2.57E-05	177.2	-53.6	5.2	35.9	22/26
AF Low Coercivity	20LH01		235.5	32.6	19.8	39.8	3/5
AF Low Coercivity	20LH02		6.1	-21.5	31.8	5.4	4/6
AF Low Coercivity	20LH03		311.6	7.8	12.7	37.3	5/5
AF Low Coercivity	20LH04		181.2	19.8	10.3	56.7	5/5
AF Low Coercivity	20LH05		343.9	40	23.7	11.3	5/5
Thermal	20LH01	3.59E-06	235	9.2	28.4	8.2	5/5
Thermal	20LH02	3.92E-05	351.5	-46.9	41.9	9.7	3/4
Thermal	20LH03	9.10E-06	264.5	-31	14.4	29	5/5
Thermal	20LH04	6.95E-06	184.4	-3.3	11.1	48.4	5/5
Thermal	20LH05	4.45E-06	20.3	-0.1	57.9	2.7	4/5
*Boars Tusk 3			178.7	-48.4	10.8	51.6	5
*Boars Tusk 4			153.6	-53	18.1	26.7	4
		$A m^{-1}$					
	BR01	1.71E-01	356.8	60.3	4.4	66	17
	BR02	2.33E-01	358.7	55.9	5.6	62	12
	BR03	1.54E-01	4	55.9	4.8	60	16
	BR04	1.81E-01	11.3	58	4.9	89	11
BR Suite Average		1.85E-01	3	58	4	501	56
* Black Rock			20.6	56.6	8.4	64.4	6

Site average NRM is the average natural remanent magnetization at each site reported in either $Am^2 kg^{-1}$ for Boars Tusk or Am^{-1} for Black Rock; a_{95} is the radius of 95% confidence cone; k is precision parameter; n/N is the number of successful samples (n) out of the total number of samples (N), where if only one number is present it is the total number of successful samples; *data from Sheriff and Shive (1980).

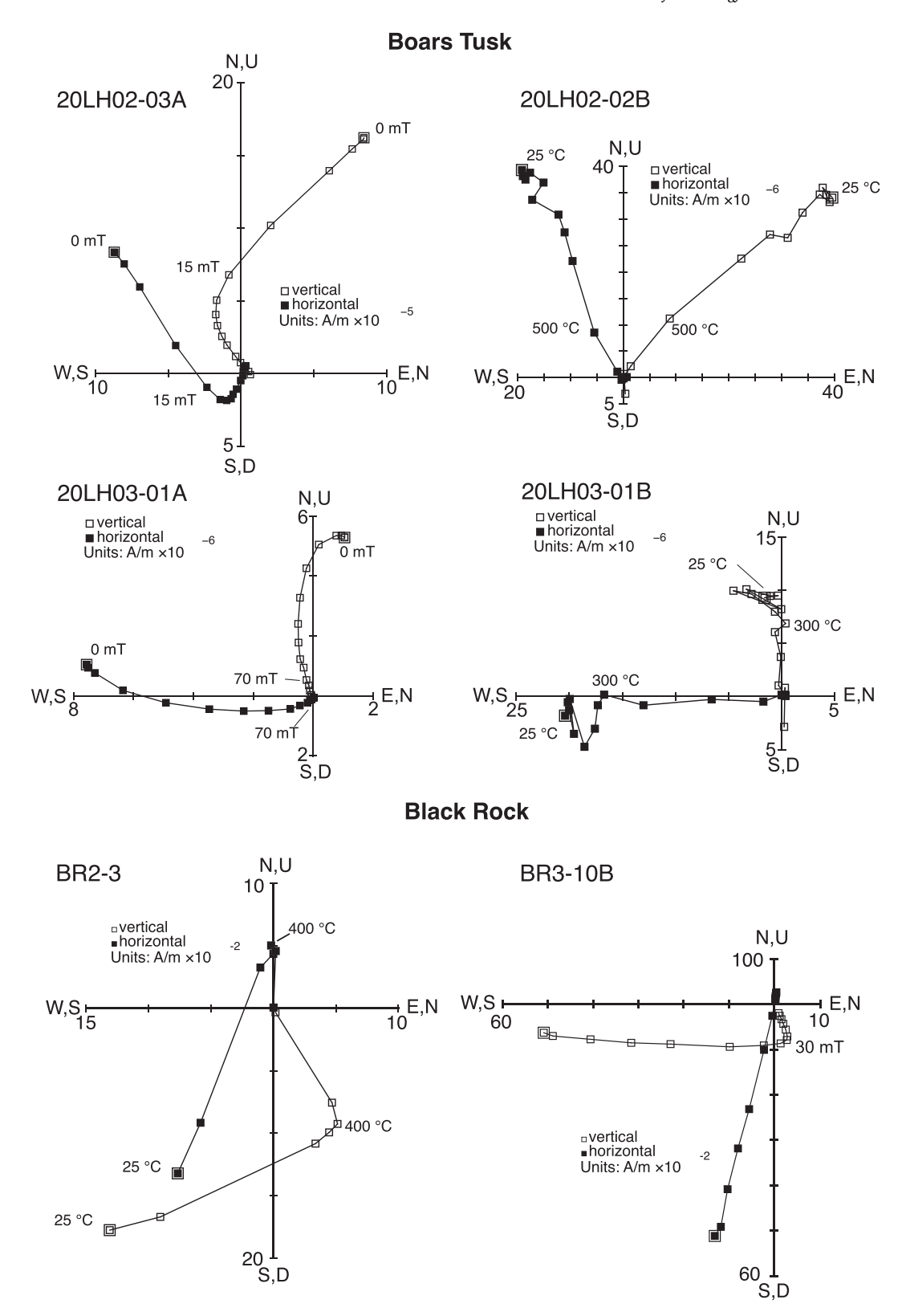


Fig. 3. Vector endpoint diagrams of alternating field and thermal demagnetization experiments for Boars Tusk dike specimens (20LH02) and breccia specimens (20LH03) and Black Rock specimens BR2–3 (thermal) and BR3-10b (AF).

accepted if individual specimen directions were accepted when the maximum angular deviation (MAD) is below 10° for AF demagnetization and 20° for thermal demagnetization. 56 of 60 specimens met the acceptance criteria. Four specimens (2 from BR01 and 2 of BR03) were not included in the mean Fisher direction calculation for having

aberrant (e.g., south and positive) directions. We suspect the presence of a secondary, possibly lightning strike related remagnetization, which totally masks the primary ChRM direction in few samples (see discussion below). Fisher mean directions were accepted when α_{95} <14° and all sites were included in site mean direction calculation. Unlike Boars

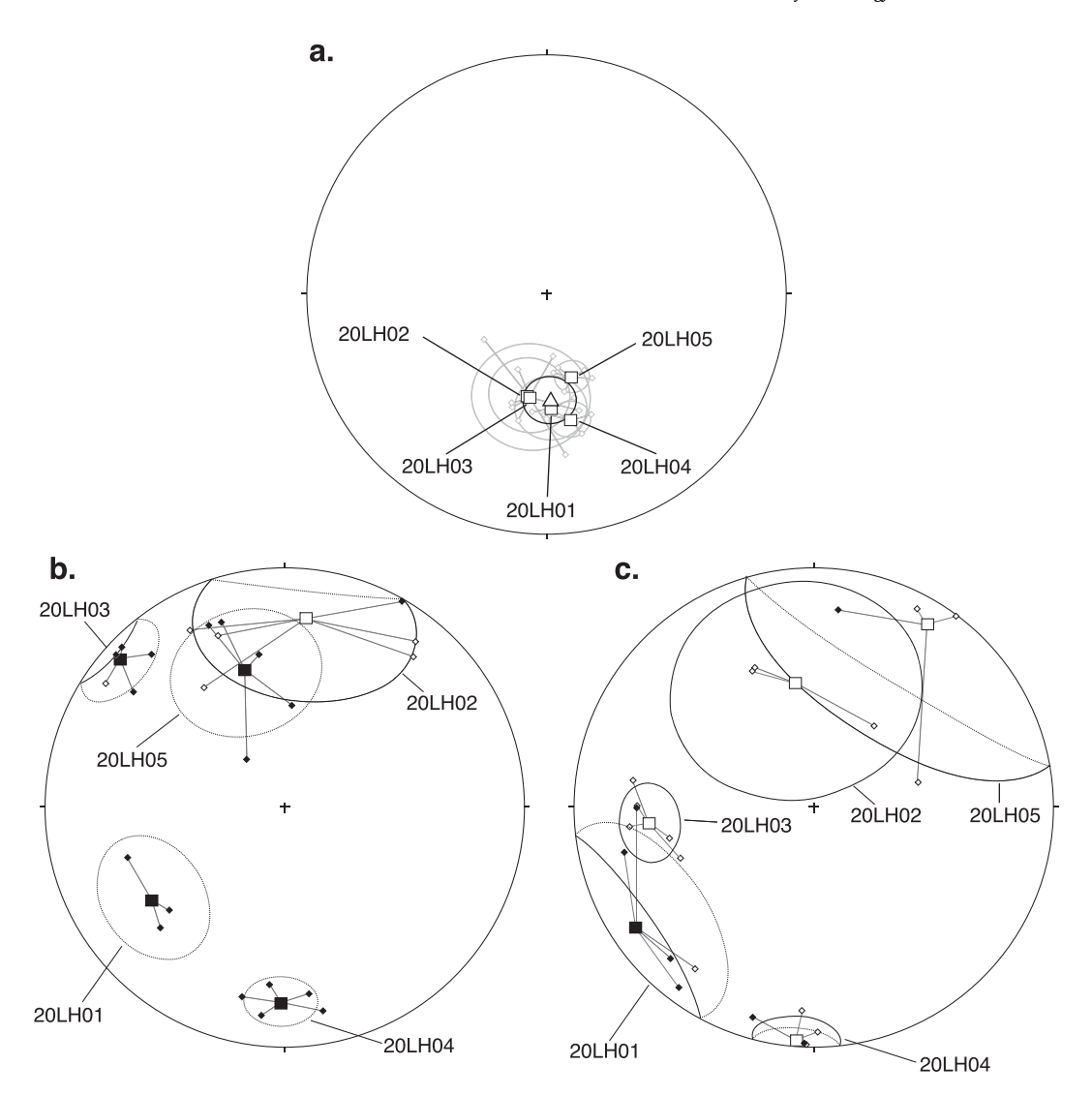


Fig. 4. Stereonets showing Boars Tusk directions obtained using (a) alternating field high coercivity, (b) alternating field low coercivity, and (c) thermal demagnetization data. Specimen directions are diamonds, site averages are boxes, and the suite average for AF high coercivity data is a triangle. Circles show α_{95} confidence limits.

Tusk, the data collected using thermal demagnetization procedures was not significantly noisier than the alternating field data. Both AF and thermal demagnetization of Black Rock samples produced a straightforward and reliable characteristic remanent magnetization at all sites. The Fisher mean declination and inclination for Black Rock is 3° and 58° , respectively. Thermal and AF demagnetization also revealed a secondary component recorded in most Black Rock specimens which was removed within the first few steps of the demagnetization protocols (by 350 °C for thermal demagnetization with a few specimens persisting to 400 °C). These secondary components are variable in direction between specimens and sites.

NRM values from Black Rock samples were comparable to those from Boars Tusk, ranging from $\sim\!\!1.5\times10^{-1}~Am^{-1}$ to $\sim\!\!2.4\times10^{-1}~Am^{-1}.$ Using a value of 2600 kg m $^{-1}$ for the density of lamproite (Chalapathi Rao, 2008) we estimated the mass normalized value of NRM for these samples at $\sim\!\!6\times10^{-5}~Am^2kg^{-1}$ to $\sim\!\!9\times10^{-5}~Am^2kg^{-1}$, values that are within an order of magnitude of those from Boars Tusk.

4.2. 40 Ar/ 39 Ar results

Initial experiments found that multi-crystal phlogopite aliquots produce $^{40}\mathrm{Ar}$ signals that were too large for the ion counting multipliers

of the Noblesse mass spectrometer. So, single-crystal 40 Ar/ 39 Ar incremental heating experiments were conducted on one sample from Boars Tusk (labeled Boars Tusk), and two samples from Black Rock (labeled BR0-6B and BR0–5C). Data from these experiments are summarized in Table 3 and shown in Fig. 5.

Boars Tusk gives a plateau age of 2500 ± 10 ka with an MSWD of 1.24. Lange et al. (2000) report a $^{40}\text{Ar/}^{39}\text{Ar}$ plateau age for Boars Tusk of 2230 \pm 30 ka from a multi-crystal phlogopite aliquot with a corresponding isochron of 2240 \pm 250 ka. They also report a whole rock age of 2190 \pm 40 ka with a corresponding isochron of 2260 \pm 160 ka.

BR04-6B gives a plateau age of 880 \pm 13 ka with an MSWD of 0.77. BR04-5C was analyzed twice. The first experiment produced a discordant spectrum; initial steps are near 850 ka and then higher temperature steps are >1.5 Ma. A second experiment on a smaller crystal gives a plateau with an imprecise age of 912 \pm 70 ka, where the plateau comprises 100% of 39 Ar released with an MWSD of 0.84. The large uncertainty is likely due to the small size of this crystal. The isochrons have intercepts that are within uncertainty of the atmospheric value. For Black Rock, Lange et al. (2000) report 40 Ar/ 39 Ar plateau and isochron ages for two samples: multi-crystal phlogopite plateau ages of 1340 \pm 60 ka and 1330 \pm 60 ka, and an isochron of 1370 \pm 140 ka. Whole rock aliquots measured by Lange et al. (2000) give plateau ages of 800 \pm 20

Table 3 40 Ar/ 39 Ar results.

	Integrated Age	Plateau Age	% 39Ar	Plateau MSWD	n	Isochron Age	Isochron MSWD	N
Sample	(ka) $\pm 2\sigma$	(ka) $\pm 2\sigma$				(ka) $\pm 2\sigma$		
Boars Tusk	2453.3 ± 16.4	2501.8 ± 11.4	78	1.24	8-14	2503.3 ± 25.6	1.45	8
BR04-6B	876.8 ± 22.7	879.9 ± 12.7	100	0.77	14/14	883.7 ± 16.9	0.81	14
BR04-5C	954.7 ± 78.9	912.5 ± 70.4	100	0.84	10-10	867.0 ± 103.4	0.77	10
	1379 ± 37.8							
*Boars Tusk phlogopite	2.23 ± 0.03	2230 ± 40	100	1.57	_	2.24 ± 0.25	1.74	-
*Boars Tusk whole rock	2560 ± 90	2190 ± 40	90	0.99	-	2260 ± 160	1.03	-
*Black Rock phlogopite 1	1.35 ± 0.07	1340 ± 60	100	0.77		1.37 ± 0.14	0.92	_
*Black Rock phlogopite 2	1.30 ± 0.06	1330 ± 60	100	1.08				
*Black Rock whole rock 1	0.80 ± 0.02	800 ± 20	100	1.65		0.78 ± 0.03	1.81	-
*Black Rock whole rock 2	0.79 ± 0.02	780 ± 20	95	1.7				

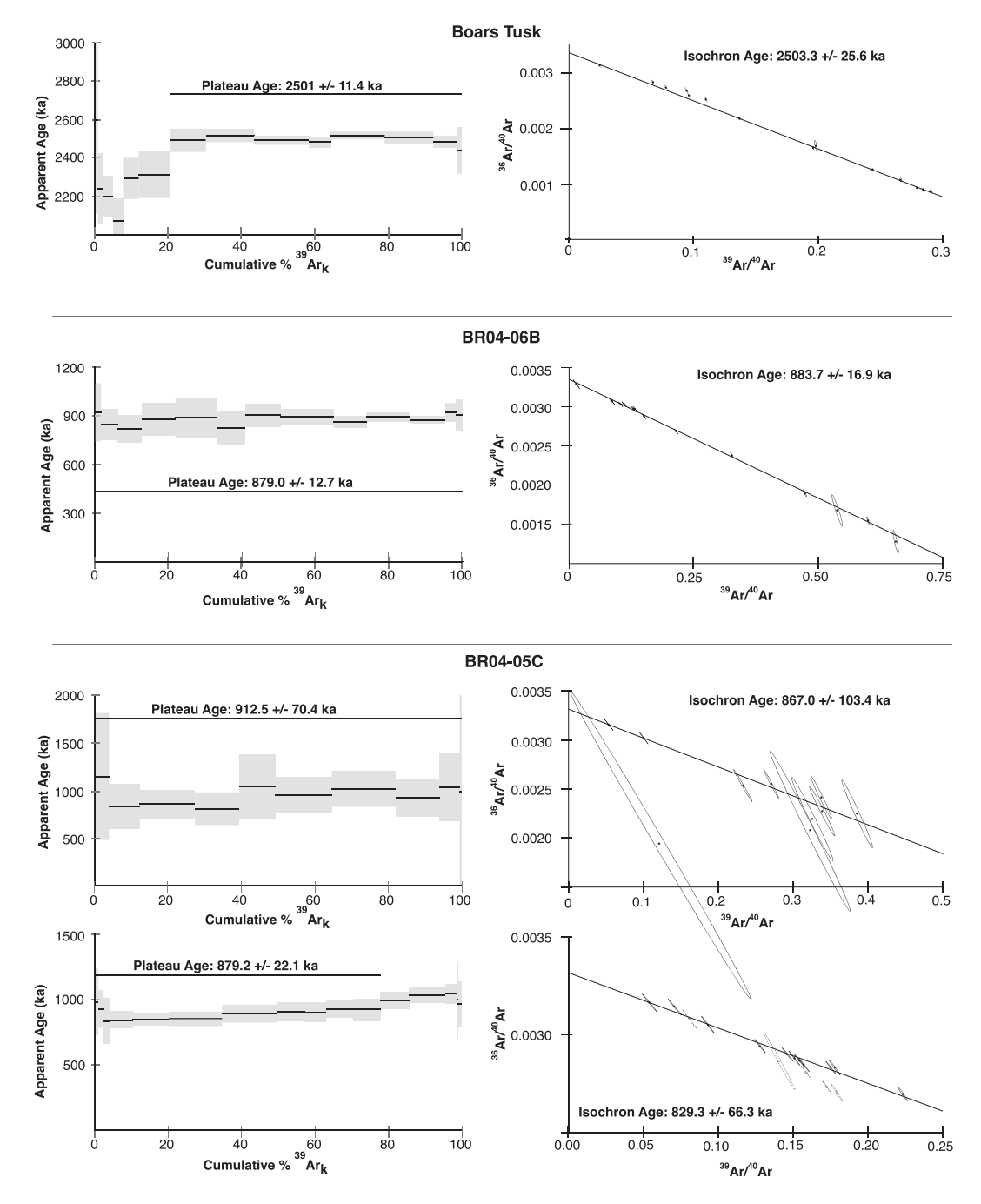


Fig. 5. Age spectra and isochron diagrams for the ages of Boars Tusk and Black Rock determined in this study.

ka and 780 \pm 20 ka, and an isochron of 780 \pm 30 ka.

The age of Boars Tusk found here is older by about 200–300 ka than proposed by Lange et al. (2000) yet this dike remains one of the oldest features in the Leucite Hills. Our plateau age (weighted mean 881 ± 12 ka) for Black Rock is younger by 100 to 400 ka than those of Lange et al. (2000). Based on a histogram of eruption volume adapted from Lange et al. (2000), our new age for Black Rock falls during the main eruptive pulse of the Leucite Hills (see below).

4.3. Magnetic characterization

4.3.1. Boars Tusk

Low-field thermomagnetic curves were near the sensitivity limit of the susceptibility meter used to collect the data, but still show that the magnetic material within these specimens has Curie temperatures between 540 °C and 612 °C (Table 4), suggesting that the primary magnetic mineral carrier is nearly pure magnetite or its partially oxidized equivalent (maghemite) (Fig. 6). Approximately half of the specimens show evidence of a secondary phase with a Néel temperature of around 670 °C, likely hematite. During cooling, lower Curie temperatures are observed for all but one specimen, with a range of 510 °C to 560 °C, suggesting some subtle alteration and perhaps growth of new magnetic minerals during heating. Most cooling curves were reversible, indicating that any magnetic mineral alteration and growth was minimal.

Hysteresis loops were dominated by paramagnetic contributions from the specimen's silicate minerals and reflect the low concentration of ferromagnetic minerals. Subtracting the paramagnetic component and stacking repeated measurements allowed a more unfettered view of the ferromagnetic behavior (Fig. 7). The breccia sample (20LH01-01 A) had a saturation magnetization (Ms) and saturation remanence (Mr) of 6.9×10^{-4} Am²kg⁻¹ and 7.7×10^{-5} Am²kg⁻¹, respectively. These were similar when compared to the M_s and M_r of the dike sample (20LH02–09B), which had values of 3.6×10^{-4} Am²kg⁻¹ and 3.4×10^{-5} Am²kg⁻¹, respectively. Coercivities for these two samples were similar, at 19.2 mT and 16.7 mT. Backfield curves also show comparable coercivities of remanence at 45.0 mT and 41.2 mT respectively. In general, it appears that the breccia samples have a slightly higher concentration of magnetic minerals, though their average grain size is similar. Because the NRM intensity of the lamproite dike is greater than that of the breccia, the efficiency of the TRM acquired by the lamproite dike must have been greater than the efficiency of remanence acquisition in the breccia.

As discussed previously, during AF demagnetization a number of dike and breccia specimens did not lose all their magnetization after high AF demagnetization steps. Some retained a high percentage of their remanence even after the 170 mT AF demagnetization step. This behavior suggests that these specimens contain a fraction of high coercivity minerals. Many of these specimens had an orange to red coloration, suggesting that hematite may be present, though ultrafine, high coercivity magnetite also remains a possibility.

4.3.2. Black Rock

Acquisition of isothermal remanent magnetization (IRM)

Table 4Curie temperature estimates.

Specimen	Curie Temp °C (heating)	Curie Temp °C (cooling)
20LH01-05_sus_air	600	547
20LH02-08_sus_air	610	544
20LH02-09_sus_air	540	510
20LH03-04_sus_air	580	526
20LH04-06_sus_air	612	540
20LH04-07_sus_air	553	535
20LH05-01_sus_air	560	560

Curie temperatures were estimated using the first derivative method after smoothing to reduce noise within the data.

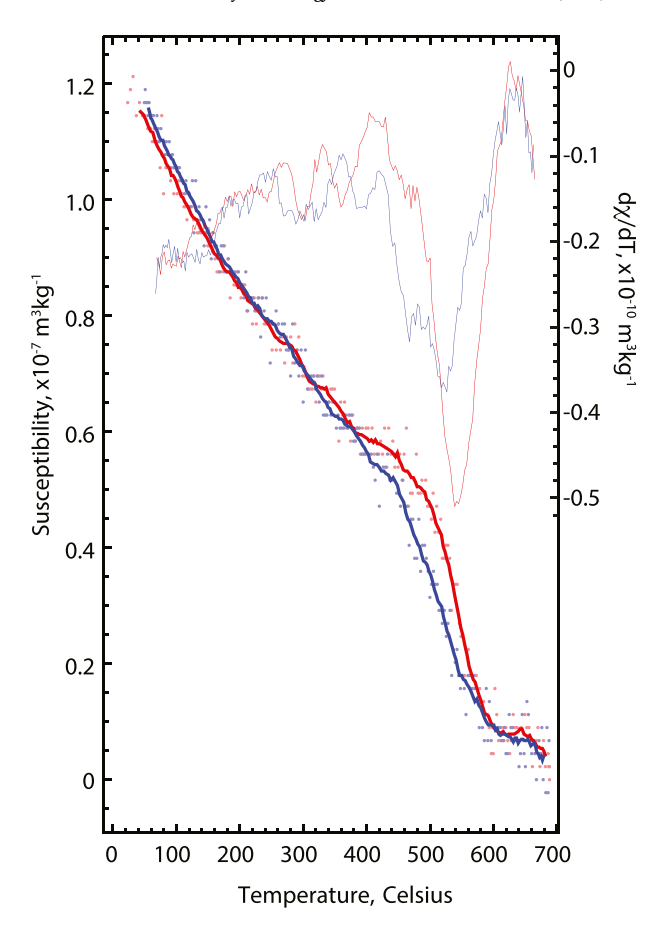


Fig. 6. Low-field thermomagnetic curve from dike sample 20LH02–09-sus-air. Raw data is displayed using light colored points and a 10-point running average was used to produce smooth lines displayed as bright colored lines. Heating data are red and cooling data are blue. The light colored lines at the top of the figure show the derivative of the susceptibility data used to determine Curie temperatures. (For interpretation of the references to colour in this figure legend, the reader is referred to the web version of this article.)

experiments were conducted on representative Black Rock specimens and are shown in Fig. 7. Remanence plateaus at applied fields of approximately 300 mT indicating that remanence is held by a cubic iron oxide, such as magnetite or its cation substituted equivalent. Thermal demagnetization experiments provide further support for the presence of magnetite in that remanence recedes to the origin after a 580 °C thermal demagnetization step. Although there are minor secondary magnetizations, there is no indication of a secondary mineral assemblage. Instead, the Black Rock samples appear to contain a largely monomineralic magnetic mineral assemblage.

4.4. Electron microprobe

4.4.1. Description of silicates

The major host minerals in the lamproite include apatite, phlogopite, hornblende, k-spar (leucite), albite and diopside. Phlogopite occurs in laths that are $100-200~\mu m$ with zoned rims and common alteration rinds (Fig. 8a,b). Zoned rims appear lighter in backscatter mode and are enriched in Fe and Ti and depleted in Mg and Al. Alteration rinds are particularly bright and occasionally penetrate the interior of phlogopite crystals. These alteration rinds are rich in Ba and S and are likely the barium sulfate mineral barite. The breccia consists primarily of clasts of lamproite ranging in size from several 10s of μm to several millimeters, and thus the breccia contains all the same minerals as the lamproite itself. More rarely, clasts from the nearby Eocene Green River Formation were incorporated into the breccia. The breccia is also highly vesicular,

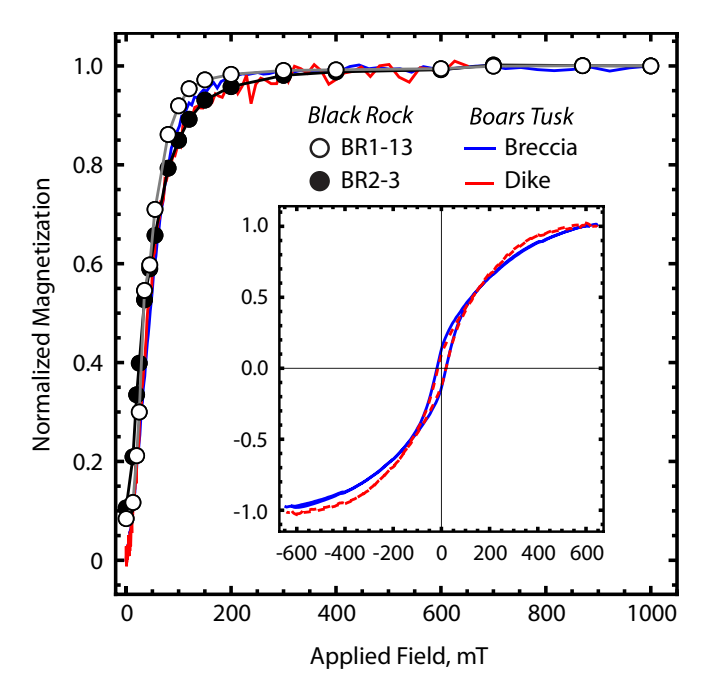


Fig. 7. IRM acquisition data for representative Black Rock and Boars Tusk specimens. The Black Rock data was collected using an impulse magnetizer and a 3-axis magnetometer, while the Boars Tusk data was originally acquired during a backfield experiment on a vibrating sample magnetometer. The agreement between the data from the two localities suggests their magnetic mineral assemblages are similar and the remanence plateau at $\sim 300~\rm mT$ indicates that the primary remanence carrier is a cubic iron oxide, such as magnetite or titanomagnetite. The inset contains normalized hysteresis loops for the Boars Tusk specimens showing similar behaviors for the dike and breccia materials.

indicating that it was volatile rich.

4.4.2. Occurrence of Fe-Ti oxides

In the lamproite and the breccia, Fe—Ti oxides are found as alteration products of phlogopite along their edges and interiors (Fig. 8a,c). These oxide alteration products have a thickness of a few to 0.5 μ m and are more extensive along the edges and cleavage planes of the phlogopite in which they reside. More rarely, in the lamproite, we found Fe—Ti oxides as exsolved inclusions within relict amphibole, which are more equant in habit than the alteration products in phlogopite crystals and range in size from 0.5 μ m to 2 μ m in diameter.

4.4.3. Fe-Ti oxide compositional measurements

The dimensions of the Fe—Ti oxides are sub-micron in scale making unambiguous compositional measurements impossible using the electron microprobe, because the excitation volume of the electron beam was always larger than the Fe—Ti oxides (Fig. 8). Compositional data for these inclusions always include traces of Si, Al, K, and Mg, which are associated with the surrounding silicate minerals. In this study we provide information about the composition of Fe—Ti oxides by comparing their measured composition to that of the silicate host. The oxides of interest contained variable amounts of Ti, some with no Ti and others with significant quantities. The relative amount of Ti did not appear to be consistent between oxides located in the same setting (interior vs exterior of phlogopite grains).

5. Discussion

5.1. Secondary magnetizations

A low coercivity component of magnetization was found in all AF

demagnetized samples from Boars Tusk and Black Rock. These components are considered secondary and are most likely due to lightning strikes for several reasons. Firstly, this component is held by a very low coercivity fraction of the sample and is removed by 15 mT. This dramatic loss of remanence is characteristic of a lightning strike and has been observed in previous studies of volcanic rocks (e.g., Cox, 1961; Tauxe et al., 2003). Secondary components from some sites are normal while others are reversed, and the declinations and inclinations of the secondary magnetizations are untenable as geomagnetic field directions given the Leucite Hills' geographic location. In addition, at Boars Tusk these secondary components are consistent in direction within each site, but not between sites, as would be expected for lightning strikes. For each site at Boars Tusk, the directions obtained from thermal demagnetization are coincident with those from the secondary component of the AF demagnetization. Grains with lower coercivities are more susceptible to acquiring a new magnetization from lightning strikes, so during alternating field demagnetization, separation of the characteristic direction from the secondary direction is possible. During thermal demagnetization, however, the unblocking temperatures of grain are influenced strongly by their compositions, making it more difficult to differentiate the two paleodirections held by similar mineralogies.

A low temperature component of magnetization was found in most thermal samples from Black Rock. These components are also considered secondary and are attributed to lightning strikes. Like the secondary components at Boars Tusk, the directions of these components do not align between sites and are untenable as geomagnetic field directions. Given that Boars Tusk and Black Rock each rise more than 100 m above an otherwise flat basin, the possibility of lightning strikes is high.

Hydrothermal activity, alternatively, does not seem like a likely cause of this secondary component. Firstly, we would expect our secondary paleodirections to be consistent with a geocentric axial dipole, something that we do not observe. In addition, due to Boars Tusk's small size and the small area within which samples were collected from Black, there would need to be more consistency in the paleodirections between sites at each locality for the heat from hydrothermal activity to impart a secondary magnetization. Hydrothermal activity also generates growth of new magnetic minerals, most notably hematite. While our samples do contain hematite, if hydrothermal activity produced it, we would expect a consistent direction to be held by the hematite in our samples, which is not observed.

5.2. Integration of findings into the Quaternary GITS

The eruptive history of the Leucite Hills Volcanic Complex encompasses much of the Quaternary and offers a rare opportunity to apply 40 Ar/ 39 Ar methods to improve the resolution of the geomagnetic instability timescale (GITS) during this period. The eruptive history of the complex is shown in Fig. 9a along with the isochron 40 Ar/ 39 Ar results from this study (Fig. 9b and the isochron and plateau ages of Lange et al. (2000) (9d and e, respectively). Figs. 9d and e also include the geomagnetic polarity of LHVC units as reported in Sheriff and Shive (1980). The most recent version of the GITS is shown in Fig. 9c. The superposition of these data allow us to rapidly identify times where the GITS appears to agree or be in conflict with existing data from the LHVC.

Paleomagnetic analyses of samples from Boars Tusk dike indicate that it was emplaced when the Earth's field was reversed. ChRMs for all samples from this study were isolated using high coercivity alternating field demagnetization steps and were uniformly reversed at all sites. These paleodirections are consistent with the two sites reported by Sheriff and Shive (1980). Our $^{40}{\rm Ar}/^{39}{\rm Ar}$ age of \sim 2500 ka broadly agrees with the \sim 2200 ka age proposed by Lange et al. (2000). The Earth's magnetic field was reversed during this interval, which coincides with the lower Matuyama Chron (C2r; Fig. 9).

The isochron age of 883 ± 16 ka for the Black Rock lavas determined here suggests that the reversed polarity coincides with the Kamikatsura excursion. Channell et al. (2020) report multi-collector mass

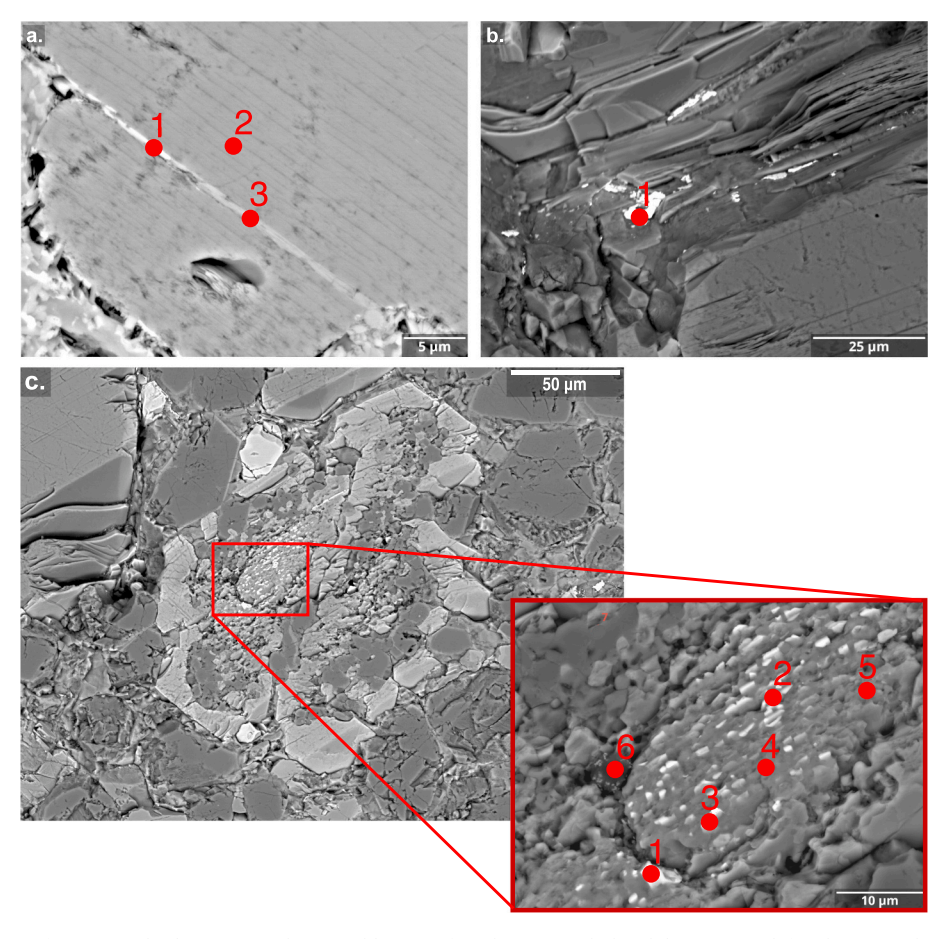


Fig. 8. (a) Backscatter image of Fe—Ti oxide alteration products in phlogopite from breccia. Light band that runs top left to bottom right and contains points 1 and 3 shows the Fe—Ti oxide. The varying brightness of the feature showed different quantities of Fe and Ti, with higher quantities at point 1 than point 3. (b) Backscatter image of barite (point 1) in breccia sample. (c) Backscatter image of Fe—Ti oxide as exsolved inclusions within a relict amphibole grain from lamproite. The larger image on the left shows the relict amphibole grain (light grey with a euhedral grain boundary). Dark grains surrounding relict amphibole include leucite and diopside. The inset shows the Fe—Ti oxides (points 1–3) and relict amphibole (points 4–6).

spectrometer 40 Ar/ 39 Ar experiments on transitionally magnetized lava flows from Tahiti and Haleakala, originally dated by Singer et al. (1999) and Coe et al. (2004), that yield comparable dates and a weighted mean age of 867 \pm 2 ka for the Kamikatsura excursion. Paleomagnetic data from astronomically-dated sediment cores suggest an age for this excursion and a global low in paleointensity during marine isotope stages 21 and 22, between about 868 and 888 ka (Channell et al., 2020). Distinct from the Kamikatsura recordings outlined above, our finding of high inclinations from the Black Rock lavas implies that during this excursion the geomagnetic field underwent a complete reversal akin to the Laschamp, Blake, Iceland Basin, Albuquerque Volcanoes/Pringle Falls excursions (Laj and Channell, 2007; Singer, 2014).

The Leucite Hills volcanic field may provide further opportunities to refine the age and geodynamo behavior associated with the Kamikatsura excursion. There are multiple features within the Leucite Hills that were emplaced at $\sim 900~{\rm ka}$, many of which provide a large percentage of the total volume of rock emplaced within the complex (Lange et al., 2000). With increased sampling, this large volume of rock may yet provide further temporal constraints and a more complete view of the geomagnetic field behavior of this excursion.

The paleomagnetic data of Sheriff and Shive (1980) and 40 Ar/ 39 Ar ages of Lange et al. (2000) suggest that several other Leucite Hills features may yet contribute to refining the Quaternary GITS. For example, the reversely magnetized Emmons Mesa yields an 40 Ar/ 39 Ar age of 996 \pm 10 ka (recalibrated to 28.201 Ma Fish Canyon sanidine; Kuiper et al., 2008) that places it coeval with the termination of the Jaramillo normal subchron (Singer, 2014; Channell et al., 2020). The reversely

magnetized Steamboat Mountain and Middle Table (Sheriff and Shive, 1980), yield $^{40}\text{Ar}/^{39}\text{Ar}$ ages of to 1812 ± 180 ka, and 1802 ± 260 ka (Lange et al., 2000; recalibrated to 28.201 Ma Fish Canyon sanidine; Kuiper et al., 2008) that should fall within the Olduvai normal subchron (Singer, 2014; Channell et al., 2020). More accurate and precise dating, coupled with modern paleomagnetic measurements from these and other Leucite Hills lavas, will help further refine the GITS and thus our understanding of geodynamo behavior during the Quaternary.

5.3. Implications for the Eruptive and geomorphic evolution of southwest Wyoming

In addition to improving the Quaternary GITS, constraining the ages of the features in the Leucite Hills would allow for a better understanding of the eruptive evolution of the volcanic field. Precise and accurate ages would create a more detailed picture of the large-scale eruptive history of the region and could clarify the impetus for volcanic activity. Increased sampling alongside more detailed field observations at individual features could help formulate emplacement histories for each feature. Updated feature ages would also create a more accurate geomorphic history of the area. Using new ages and similar procedures to Lange et al. (2000) new erosion rates could be calculated for the area. A precise age for each feature would also create tie points that could be used to address regional scale geomorphologic questions, such as the timing of integration of the Colorado River basin.

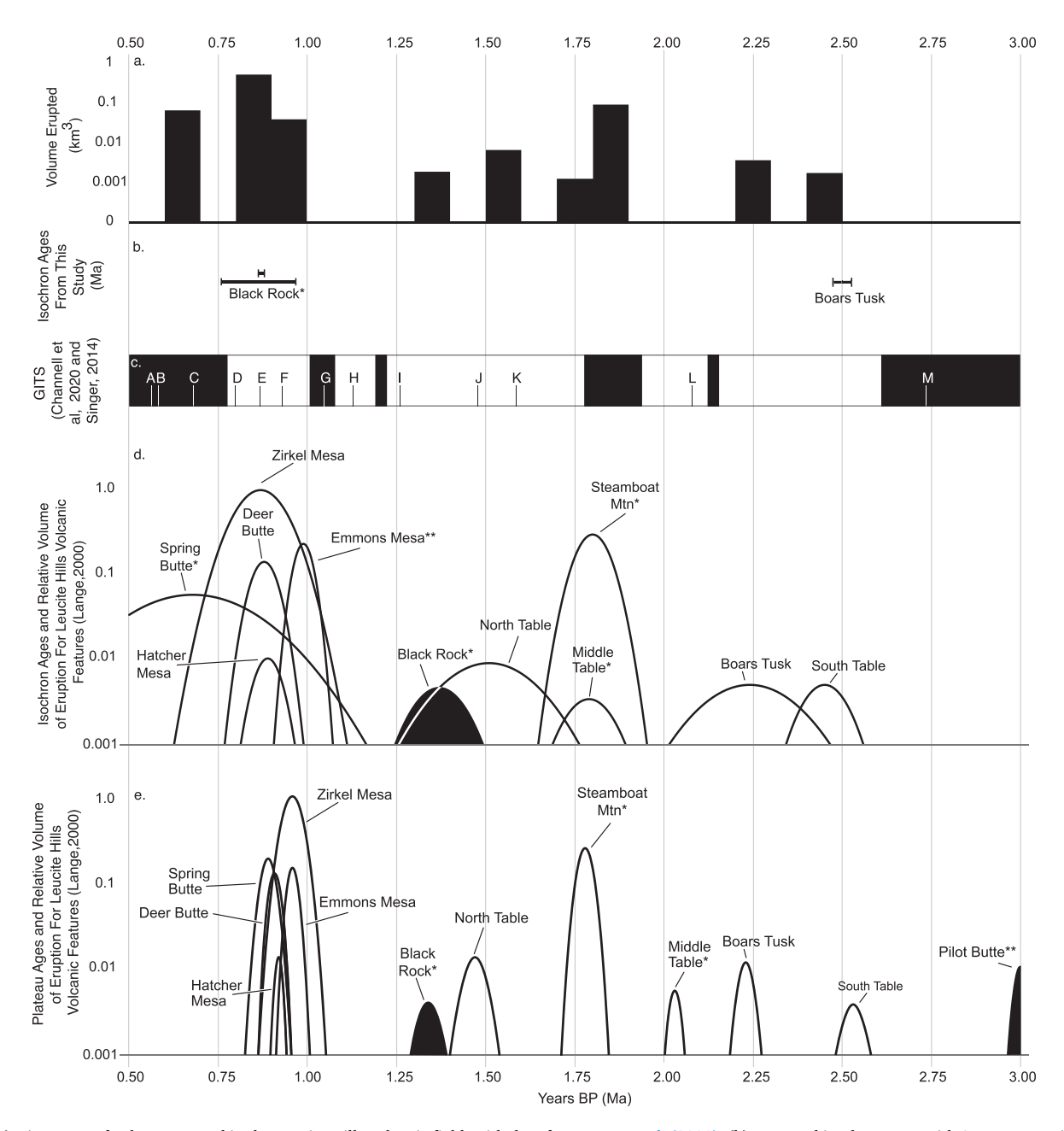


Fig. 9. (a) Histogram of volume erupted in the Leucite Hills volcanic field, with data from Lange et al. (2000). (b) Reported isochron ages with 2σ error margins from this study. (c) The geomagnetic instability timescale from Singer (2014) and Channell et al., 2020. Geomagnetic excursions are shown as small lines and are labeled A-M. Here, we list the excursion associated with each line: A, Big Lost; B, La Palma; C, Osaka Bay; D, M/B Precursor; E, Kamikatsura; F, Santa Rosa; G, Intra-Jaramillo; H, Punaruu; I, Bjorn; J, Gardar; K, Gilsa; L, Huckleberry Ridge; M, Porcupine. (d) and (e) The timing and relative eruption volume for Leucite Hills volcanic features. Each feature is represented by a normal curve, whose position and spread represents the isochron age and its error, respectively. The height of each curve represents the volume erupted for each feature relative to Zirkel Mesa, the largest by volume. Curves which are filled in have a reported geomagnetic polarity that is normal, and all others are reversed. Each curve is labeled to specify the associated volcanic feature. *Feature's reported polarity (Sheriff and Shive, 1980) does not match the GITS. *Feature's reported ages (Lange et al., 2000) lie on the boundary between 2 chrons on the GITS.

6. Conclusions

Our paleomagnetic and 40 Ar/ 39 Ar findings from the Leucite Hills volcanic field add new information regarding the Quaternary GITS. New rock-magnetic data from Boars Tusk reveal these unique rocks to be magnetically weak, but generally good paleomagnetic recorders. New 40 Ar/ 39 Ar data from single phlogopite crystals from Boars Tusk give an age of ~ 2500 ka, and new paleomagnetic data confirms the reversed paleomagnetic direction found by Sheriff and Shive (1980), implying eruption during the lower Matuyama reversed chron. 40 Ar/ 39 Ar experiments on single phlogopite crystals from Black Rock yield an isochron

age of 883 \pm 16 ka. Coupled with new paleomagnetic data, this age implies that the Black Rock lavas record a polarity excursion, as proposed by Lange et al. (2000). The age corresponds with the Kamikatsura excursion most recently confined to between 888 and 867 ka (Channell et al., 2020). Importantly, the Black Rock lavas cooled during the Kamikatsura excursion when the field was fully reversed, leading to a high normal inclination thereby adding to a list of several excursions during which the geodynamo produced full, but very brief, reversals of polarity. The Leucite Hills volcanic field offers further opportunities to refine the Quaternary GITS, and improve our understanding of the eruptive and geomorphic evolution of the area.

Author statement

Josie T. Welsh: Investigation, Formal Analysis, Writing- Original draft preparation, Visualization, Data curation. Joshua M. Feinberg: Conceptualization, Methology, Software, Formal Analysis, Data curation, Writing- Original draft preparation, Writing- Review & Editing, Visualization, Supervision, Project Administration. Emma Schneider: Investigation, Supervision. Josep M. Pares: Conceptualization, Investigation, Formal Analysis, Writing- Review & Editing. Brian R. Jicha: Investigation, Formal Analysis, Writing- Review & Editing, Visualization, Validation. Bradley S. Singer: Writing- Reviewing and Editing. Alan R. Carroll: Writing- Reviewing and Editing.

Declaration of Competing Interest

The authors declare that they have no known competing financial interests or personal relationships that could have appeared to influence the work reported in this paper.

Data availability

Links to data used in the study are included in the Acknowledgements section.

Acknowledgements

This is IRM publication #2203. Measurement-level magnetic data associated with Boars Tusk and site-level magnetic data associated with Black Rock can be found on the MagIC Database at (doi:https://doi.org/10.7288/V4/MAGIC/19666). All data can be found in the DRUM Repository at: doi.org/10.13020/929v-p033. Part of this work was performed at the Institute for Rock Magnetism (IRM) at the University of Minnesota. The IRM is a US National Multi-user Facility supported through the Instrumentation and Facilities program of the National Science Foundation, Earth Sciences Division, and by funding from the University of Minnesota. Singer thanks the NSF Geophysics program for supporting the WiscAr lab and a University of Wisconsin-Madison Vilas Professorship that enabled the dating experiments.

We thank Dario Bilardello, Maxwell Brown, and Peat Solheid for help with data acquisition, processing, and troubleshooting in the IRM. Bryan Wathen is thanked for his assistance with sample preparation and handling in the WiscAr Laboratory. We thank Ken Kodama and an anonymous reviewer for helpful comments that improved this manuscript, as well as Sonia Calvari for gracefully managing the peer review process.

The University of Minnesota is built on the ancestral lands of the Wahpekute band that was ceded to the United States by the Treaty of Traverse des Sioux in July of 1851, in an agreement that was not paid in full. The University has also benefited from Chippewa and Dakota (Mede-wakanton, Wahpekuta, Wahpeton and Sisseton Bands) land ceded by treaty and given to the University of Minnesota via the Morrill Act. Due to its land-grant status, the infrastructure, financial foundations, and faculty, students, and staff at the University of Minnesota all continue to benefit directly from these ceded lands, and we wish to acknowledge this support in our research.

References

- Bird, P., 1984. Laramide crustal thickening event in the Rocky Mountain foreland and Great Plains. Tectonics 3, 741–758.
- Cande, S.C., Kent, D.V., 1992. A new geomagnetic polarity time scale for the late cretaceous and Cenozoic. J. Geophys. Res. Solid Earth 97 (B10), 13917–13951.
- Cande, S.C., Kent, D.V., 1995. Revised calibration of the geomagnetic polarity timescale for the late cretaceous and Cenozoic. J. Geophys. Res. Solid Earth 100 (B4), 6093–6095.
- Carmichael, I.S.E., 1967. The mineralogy and petrology of the volcanic rocks from the Leucite Hills. Wyoming: Contrib. Mineral. Petrol. 15, 24–66. https://doi.org/ 10.1007/BF01167214.

- Chalapathi Rao, N.V., 2008. In: Rajesh, K., Srivastava, C.H. Sivaji, Rao, N.V. Chalapathi (Eds.), Petrophysical Properties of Indian Kimberlites, Lamproites and Lamprophyres: Indian Dykes: Geochemistry, Geophysics and Geochronology. © 2008, Narosa Publishing House Pvt. Ltd., New Delhi, India.
- Channell, J.E.T., Singer, B.S., Jicha, B.R., 2020. Timing of Quaternary geomagnetic reversals and excursions in volcanic and sedimentary archives. Quat. Sci. Rev. 228, 106114 https://doi.org/10.1016/j.quascirey.2019.106114.
- Coe, R.S., Singer, B.S., Pringle, M.S., Zhao, X., 2004. Matuyama–Brunhes reversal and Kamikatsura event on Maui: paleomagnetic directions, ⁴⁰Ar/ ³⁹Ar ages and implications. Earth Planet. Sci. Lett. 222 (2), 667–684. https://doi.org/10.1016/j.epsl 2004.03.003
- Cox, A., 1961. Anomalous remanent magnetization of basalt: U.S. Geol. Surv. Bull. 1083-E, 131–160. https://doi.org/10.3133/b1083E.
- Cross, C.W., 1897. Igneous rocks of the leucite hills and pilot butte, wyoming. Am. J. Sci. s4-4, 115–141. https://doi.org/10.2475/ajs.s4-4.20.115.
- Dunlop, D.J., Özdemir, Ö., 1997. Rock magnetism: fundamentals and frontiers: cambridge. In: Cambridge University Press, Cambridge Studies in Magnetism. https://doi.org/10.1017/CBO9780511612794.
- Eggler, D.H., Meed, J.K., Welt, F., Dudéls, F.O., Furlong, K.P., Mccallum, M.E.,
 Carlson, R.W., Drezler, J.W., Larson, E.E., 1988. Tectonomagmatism of the Wyoming
 Province, Cenozoic Volcanism in the Southern Rocky mountains revisited: a tribute
 to Rudy C. Epis: part 3. In: The Colorado School of Mines Quarterly, 88, pp. 25–40.
- Hausel, W.D., 2006. Geology and geochemistry of the leucite hills volcanic field (2006): Wyoming State Geological Survey, p. 71.
- Houston, R.S., Erslev, E.A., Frost, C.D., Karlstrom, K.E., Page, N.J., Zientek, J.L., Reed, J.
 C., Snyder, G.L., Worl, R.G., Bryant, B., Reynolds, M.W., Peterman, Z.E., 1993. The
 Wyoming Province. In: Reed, J.C. (Ed.), Precambrian: Conterminous U.S., Geology of
 North America, C-2. Geological Society of America, pp. 121–170.
- Jackson, M., Solheid, P., 2010. On the quantitative analysis and evaluation of magnetic hysteresis data. Geochem. Geophys. Geosyst. 11 (4) https://doi.org/10.1029/ 2009GC002932.
- Jicha, B.R., Singer, B.S., Sobol, P., 2016. Re-evaluation of the ages of 40Ar/39Ar sanidine standards and supereruptions in the western U.S. using a Noblesse multi-collector mass spectrometer. Chem. Geol. 431, 54–66. https://doi.org/10.1016/j. chemgeo.2016.03.024.
- Kirschvink, J.L., 1980. The least-squares line and plane and the analysis of palaeomagnetic data. Geophys. J. R. Astron. Soc. 62 (3), 699–718. https://doi.org/ 10.1111/j.1365-246X.1980.tb02601.x.
- Kuiper, K.F., Deino, A., Hilgen, F.J., Krijgsman, W., Renne, P.R., Wijbrans, A.J., 2008. Synchronizing rock clocks of Earth history. Science 320 (5875), 500–504.
- Laj, C., Channell, J.E., 2007. Treatise on Geophysics. In: Geomagnetic excursions. Geomagnetism, 5.10, pp. 373-416.
- Lange, R.A., Carmichael, I.S.E., Hall, C.M., 2000. ⁴⁰Ar/³⁹Ar chronology of the Leucite Hills, Wyoming: eruption rates, erosion rates, and an evolving temperature structure of the underlying mantle. Earth Planet. Sci. Lett. 174, 329–340. https://doi.org/ 10.1016/S0012-821X(99)00267-8.
- Lipman, P.W., Burchfiel, B.C., Oliver, J.E., Silver, L.T., 1980. Cenozoic volcanism in the western United States. In: Implication for Continental Tectonics, Continental Tectonics. National Academy of Science, Washington, DC, pp. 161–174.
- Lurcock, P.C., Wilson, G.S., 2012. PuffinPlot: A versatile, user-friendly program for paleomagnetic analysis: Geochemistry. Geophysics, Geosystems 13. https://doi.org/ 10.1029/2012GC004098.
- Maxbauer, D.P., Feinberg, J.M., Fox, D.L., 2016. MAX UnMix: A web application for unmixing magnetic coercivity distributions. Comput. & Geosci. 95, 140–145. https://doi.org/10.1016/j.cageo.2016.07.009.
- Mirnejad, H., Bell, K., 2006. Origin and source evolution of the leucite hills lamproites: evidence from Sr-Nd-Pb-O isotopic compositions. J. Petrol. 47, 2462–2489. https://doi.org/10.1093/petrology/egl051.
- Ogden, P.R., 1979. The Geology, Major Element Geochemistry, and Petrogenesis of the Leucite Hills Volcanic Rocks. University of Wyoming, Wyoming [Ph.D.], p. 137. http://www.proquest.com/docview/303011612/citation/335D151C553E45F5PQ/1 (accessed June 2021).
- Schultz, A.R., Cross, W., 1912. Potash-bearing rocks of the Leucite Hills, Sweetwater County, 512. Wyoming: Government Printing Office Bulletin USGS Numbered Series. https://doi.org/10.3133/b512.
- Sheriff, S.D., Shive, P.N., 1980. Paleomagnetism of the Leucite Hills volcanic field, southwestern Wyoming. Geophys. Res. Lett. 7, 1025–1028. https://doi.org/ 10.1029/GL007i012p01025.
- Singer, B.S., 2014. A Quaternary geomagnetic instability time scale. Quat. Geochronol.
- 21, 29–52.
 Singer, B.S., Hoffman, K.A., Chauvin, A., Coe, R.S., Pringle, M.S., 1999. Dating transitionally magnetized lavas of the late Matuyama Chron: toward a new ⁴⁰Ar/³⁹Ar timescale of reversals and events: Journal of Geophysical Research: Solid. Earth 104, 679–693. https://doi.org/10.1029/1998JB900016.
- Tauxe, L., Constable, C., Johnson, C.L., Koppers, A.A.P., Miller, W.R., Staudigel, H., 2003. Paleomagnetism of the southwestern USA recorded by 0-5 Ma igneous rocks. Geochem. Geophys. Geosyst. 4 (8802) https://doi.org/10.1029/2002GC000343.
- Woolley, A.R., Bergman, S.C., Edgar, A.D., Bas, M.J.L., Mitchell, R.H., Rock, N.M.S., Smith, B.H.S., 1996. Classification of lamprophyres, lamproites, kimberlites, and the kalsilitic, melilitic, and leucitic rocks. Can. Mineral. 34, 175–186.
- Zijderveld, J.D.A., 1967. The natural remanent magnetizations of the exeter volcanic traps (Permian, Europe). Tectonophysics 4 (2), 121–153. https://doi.org/10.1016/ 0040-1951(67)90048-0.